

Influence of Tetrapropylammonium and Ethylenediamine Structure-Directing Agents on the Framework Al Distribution in B-Al-MFI **Zeolites**

Young Gul Hur,[†] Philip M. Kester,[†] Claire T. Nimlos, YoonRae Cho, Jeffrey T. Miller,[©] and Rajamani Gounder*

Charles D. Davidson School of Chemical Engineering, Purdue University, 480 Stadium Mall Drive, West Lafayette, Indiana 47906, United States

Supporting Information

ABSTRACT: We report synthetic protocols to independently influence composition and crystallite sizes of MFI zeolites, properties that contribute to Thiele moduli, and the proximity of Al heteroatoms at fixed composition (Si/Al ~ 50). Crystallite sizes decrease with the addition of noncatalytic B heteroatoms in B-Al-MFI zeolites. Using only tetra-n-propylammonium (TPA+) as a structure-directing agent (SDA) leads to occlusion of one TPA+ per channel intersection and a finite percentage of framework Al atoms (20-40%) in proximal configurations. In contrast, using mixtures of ethylenediamine (EDA) and TPA+ (EDA/TPA+ = 15) leads to incorporation of EDA that displaces some TPA+ and to nearly all (>95%) Al in isolated configurations. These

findings indicate how adding B and EDA to zeolite synthesis solutions provides a route to crystallizing MFI zeolites of similar composition but with framework Al distributed at varying relative proximity, or with similar Al distributions but different diffusion path lengths.

1. INTRODUCTION

Zeolites are a class of microporous solid acid catalysts that influence reactivity by regulating the access and egress of reactants and products within intracrystalline pores via shape selectivity concepts¹ and by stabilizing confined reactive intermediates and transition states via van der Waals interactions with lattice oxygen atoms.^{2,3} MFI zeolites⁴ are often used in catalytic hydrocarbon upgrading routes (e.g., methanol-to-olefins (MTO)⁵ and olefin oligomerization^{6,7}) because their three-dimensional pore interconnectivity attenuates deactivation from micropore blocking by carbonaceous deposits compared to one-dimensional zeolites (e.g., MOR) or zeolites with larger differences between their largest cavity diameters and diffusion-limiting apertures (e.g., ERI).8 Carbonaceous deposits formed during propene oligomerization on MFI zeolites (473 K) that cause deactivation become increasingly aromatic in nature with increasing crystallite size, because secondary reactions on Brønsted acid sites that produce aromatics become more prevalent with increasing intracrystalline residence time.8 The size of zeolite crystallites and the volumetric density of Brønsted acid sites contribute to a characteristic diffusion parameter (Ψ , eq 1), found in Thiele modulus expressions that relate reaction and diffusion rates within porous catalysts.

$$\Psi = [H^+]L^2 \tag{1}$$

The preferential increase in intracrystalline residence times of bulky intermediates, imparted by the diffusion parameter, leads to increases in selectivity toward products formed from these larger reactive intermediates. Such phenomena are reflected in the increased selectivity to ethene produced from substituted aromatic intermediates during MTO10,111 and to products of secondary β -scission of longer hydrocarbon intermediates during propene oligomerization¹² in MFI zeolites.

Product selectivities in such reactions can thus be influenced by synthetic methods to vary the diffusion parameter of zeolite crystallites, either by changing the density of Brønsted acid protons via framework Al or the characteristic crystallite size, yet these two material properties are generally correlated in conventional hydrothermal synthesis. Linear crystal growth rates have been shown to decrease with increasing Al content in MFI synthesis solutions, 13,14 although the size of the resulting crystallites depends on the alkalinity of the synthesis medium because of competition between crystal growth and dissolution, which are both catalyzed by hydroxide anions.¹²

March 28, 2019 Received: Revised: June 5, 2019 Accepted: June 10, 2019 Published: June 10, 2019

11849

Hydroxide anions are often present in structure directing agent (SDA) precursors, including tetra-*n*-propylammonium (TPA⁺) and Na⁺ cations that are commonly used in MFI synthesis. In the case of MFI zeolites, TPA+ cations form clathrate structures with water molecules in solution, which are isomorphously replaced by silicate precursors with a Si/ TPA⁺ ratio of ~24, corresponding to one TPA⁺ per intersection in MFI.¹⁵ Al incorporation into the lattice is proposed to occur via aluminate substitution into TPA+ clathrates and S_N2-type nucleophilic attack of a deprotonated oxygen within a silicate tetrahedron on an aluminate species, to form Al-O-Si bonds. 16 Other SDAs (e.g., Na+) compete with TPA⁺ to balance the charge in anionic aluminate species¹⁶ and may influence the siting of Al at crystallographically unique locations in MFI zeolite frameworks.¹⁷ Therefore, characteristic diffusion lengths and framework Al siting in MFI zeolites depend on the identity and quantity of organic and inorganic precursors in synthetic solutions, which provide alternative strategies to independently influence material properties that define characteristic diffusion parameters of zeolites.

Indeed, several alternative methods have been studied previously to influence either the size and morphology of zeolite crystallites or the siting of Al heteroatoms within their frameworks. Alcohol and amine additives (termed "zeolite growth modifiers", or ZGMs) in hydrothermal synthesis solutions bind to certain crystallite facets of silicalite-1 (Si-MFI), thereby inhibiting crystal growth in certain directions, which decreases the size of crystalline products and influences their aspect ratios. Ethylenediamine (EDA) is one such additive and has also been used as a template for borosilicate^{20,21} and boroaluminosilicate²² MFI compositions. Competition between B and Al for incorporation into MWW frameworks has been implicated to bias Al siting away from Tsite locations in larger voids, which are more prone to deactivation during MTO catalysis.²³ Brønsted acidic protons that compensate for B heteroatoms are catalytically irrelevant in comparison to those compensating framework Al, 24 because the former have ~70 kJ mol⁻¹ higher deprotonation energies;² therefore, such protons do not contribute to zeolite characteristic diffusion parameters. We have recently reported the synthesis of B-Al-MFI zeolites using mixtures of organic TPA+ and EDA molecules to independently influence crystallite size (\sim 0.3–10 μ m) and bulk Al content (Si/Al > 70).²² Here, we build upon this prior work to synthesize B-Al-MFI zeolites from mixtures containing TPA⁺ as the only organic SDA and from mixtures of TPA+ and EDA as co-SDAs, to provide evidence that this strategy can enable independently varying the fraction of Al in proximal or isolated locations of MFI (at fixed Si/Al) in samples with different characteristic diffusion parameters.

2. METHODS AND MATERIALS

2.1. Synthesis of B–Al–MFI Zeolites. Two methods were used to synthesize B–Al–MFI zeolites of varying elemental composition (Si/B and Si/Al ratio). In the first route, B–Al–MFI–TPA zeolites were synthesized as reported by Zhu et al. 26 using tetra-n-propylammonium (TPA $^+$) as the organic SDA. Synthesis gels comprising a molar ratio of X H $_3$ BO $_3$ /0.01 Al $_2$ O $_3$ /1 SiO $_2$ /0.32 TPAOH/30.45 H $_2$ O were prepared, where X was varied from 0 to 0.4. The synthesis procedure involved adding aluminum hydroxide (Al(OH) $_3$, 99 wt %, SPI Pharma), tetra-n-propylammonium hydroxide (TPAOH, 40 wt %, Alfa Aesar), and boric acid (H $_3$ BO $_3$,

99.5 wt %, Sigma-Aldrich) to deionized H_2O (18.2 $M\Omega$) in a perfluoroalkoxy alkane (PFA) container (Savillex Corp.) and stirring the solution under ambient conditions for 0.25 h. Next, fumed silica (SiO₂, 99 wt %, Cabot) was added to the solution, and the mixture was stirred under ambient conditions for 2 h to homogenize the contents. The synthesis solution was then transferred to a 45 mL Teflon-lined stainless-steel autoclave and placed in a forced convection oven at 443 K and rotated at 50 rpm for 168 h. These B–Al–MFI samples are referred as B–Al–MFI–TPA (a, b) to denote that TPA⁺ was the only organic SDA present during synthesis, where a is the Si/B molar ratio and b is the Si/Al molar ratio used in the synthesis solution.

In the second route, B-Al-MFI-EDA zeolites were synthesized by adapting methods reported in Kester et al.²² that use ethylenediamine (EDA) and TPA+ as organic SDAs during crystallization. Synthesis gels comprising a molar ratio of 0.3 EDA/X H₃BO₃/Y Al₂O₃/1 SiO₂/0.02 TPAOH/10.2 H_2O were prepared, where X was varied from 0-0.4 and Y from 0-0.01. The synthesis procedure involved adding EDA (99.5 wt %, Sigma-Aldrich) and H₃BO₃ (99.5 wt %, Sigma-Aldrich) to deionized H_2O (18.2 $M\Omega$) in a PFA container and stirring the solution under ambient conditions for 0.25 h. Next, aluminum nitrate nonahydrate (Al(NO₃)₃, 98 wt %, Alfa Aesar) and TPAOH (40 wt %, Alfa Aesar) were added to the EDA-containing solution, and the mixture was stirred under ambient conditions for 0.25 h to homogenize the contents. Finally, colloidal silica (Ludox HS-40, 40 wt %, Sigma-Aldrich) was added to the mixture and stirred for 2 h under ambient conditions. The synthesis solution was then transferred to a 45 mL Teflon-lined stainless-steel autoclave and placed in a forced convection oven at 448 K and rotated at 50 rpm for 120 h. These B-Al-MFI samples are denoted as B-Al-MFI-EDA (a, b) to denote that EDA was also present as an organic SDA in the synthesis solution, where a is the Si/B molar ratio and bis the Si/Al molar ratio used in the synthesis.

2.2. Preparation of Cation-Exchanged Zeolites. Zeolite products were recovered from autoclaves and washed with deionized water (18.2 M Ω) and acetone (Sigma-Aldrich, 99.9 wt %) in alternating steps until the pH of the supernatant remained constant between washes. Solids then were recovered via centrifugation, dried at 373 K under stagnant air for 24 h, and then treated in flowing dry air (1.67 cm³ s⁻¹ g_{cat}, 99.999% UHP, Indiana Oxygen) at 853 K (0.0167 K s⁻¹) for 10 h. B-Al-MFI zeolites were converted to NH₄-form via aqueous phase ion-exchange using 150 cm³ of a 1.0 M NH₄NO₃ solution (8.0 wt % in deionized water, 99.9 wt %, Sigma-Aldrich), followed by washing four times with deionized water (70 cm³ per g solids). NH₄-form zeolites were converted to their proton form via treatment in flowing dry air (1.67 cm³ s⁻¹ g_{cat}⁻¹, 99.999% UHP, Indiana Oxygen) at 773 K (0.0167 K s⁻¹) for 4 h. Na-form B-Al-MFI zeolites were prepared by aqueous phase ion-exchange using 150 cm³ of a 1.0 M NaCl solution (5.8 wt % in deionized water, 99.9 wt %, Sigma-Aldrich) per gram of zeolite for 24 h under ambient conditions, followed by washing the solids four times with deionized water (70 cm³ per g solids). Na-form zeolites were recovered using centrifugation, dried at 373 K under stagnant air for 24 h, and then treated in flowing dry air (1.67 cm 3 s $^{-1}$ g $_{cat}^{-1}$, 99.999% UHP, Indiana Oxygen) at 773 K (0.0167 K s $^{-1}$) for 4 h. Naform B-Al-MFI zeolites were converted to their Co²⁺ form by ion-exchange by stirring samples with 0-0.5 M Co(NO₃)₂ solutions (0-9.1 wt % in deionized water, 99 wt %, SigmaAldrich) at 293–353 K for 24 h. Samples were then washed four times with deionized water until the pH was constant between washes, recovered via centrifugation, and dried at 373 K under stagnant air for 24 h. Co-zeolites were then treated in flowing dry air (1.67 cm 3 s $^{-1}$ g $_{cat}^{-1}$, 99.999% UHP, Indiana Oxygen) at 773 K (0.0167 K s $^{-1}$) for 4 h.

2.3. Zeolite Characterization. Powder X-ray diffraction (XRD) patterns collected using a Rigaku SmartLab X-ray diffractometer with a Cu $K\alpha$ source operated at 1.76 kW. Approximately 0.01 g of zeolite was loaded into a zero-background, low dead-volume sample holder (Rigaku), and diffraction patterns were measured from 4–40° with a step size of 0.01° and a scan rate of 0.0167° s⁻¹. The MFI topology was confirmed via comparison with reference patterns.²⁷

Micropore volumes were calculated from N_2 adsorption isotherms measured at 77 K using a Micromeritics ASAP 2020 surface area and porosity analyzer. B–Al–MFI samples (0.04–0.06 g, sieved to 180–250 μ m) were degassed by heating to 393 K (0.167 K s⁻¹) under vacuum (5 μ mHg) for 2 h, then heating to 623 K (0.167 K s⁻¹) under vacuum (<5 mmHg) and holding for 9 h. The linear volumetric uptake of N_2 at 0.05–0.35 P/P_0 was extrapolated to zero pressure to estimate micropore volumes.

Elemental analysis of Al and Co in B–Al–MFI zeolites were performed via atomic absorption spectroscopy (AAS) using a PerkinElmer Model AAnalyst 300 atomic absorption spectrometer. Samples were prepared by dissolving 0.04–0.06 g of solid in 2 g of hydrofluoric acid (48 wt %, Alfa Aesar) and allowed to sit overnight, then diluted with 50 g of deionized water (18.2 M Ω). Radiation sources with wavelengths of 309.3 and 240.7 nm were used to measure absorbances for Al and Co in a reducing acetylene/nitrous oxide flame and oxidizing acetylene/air flame, respectively. Elemental compositions were calculated using calibration curves generated from standard solutions. B contents in B–Al–MFI zeolites were determined by inductively coupled plasma—optical emission spectroscopy (ICP-OES, Galbraith Laboratories).

²⁷Al and ¹¹B magic angle spinning nuclear magnetic resonance (MAS NMR) spectra were recorded under ambient conditions on the H-form of B–Al–MFI zeolites to probe the coordination of Al and B heteroatoms. Spectra were recorded on a Chemagnetics CMX-Infinity 400 spectrometer in a widebore 9.4 T magnet (Purdue Interdepartmental NMR Facility). Prior to collecting NMR spectra, samples were hydrated for >48 h in a desiccator containing a saturated potassium chloride (KCl) solution. Spectra were normalized such that the maximum intensity in each spectrum is unity.

Ammonia temperature-programmed desorption (TPD) experiments were performed using a Micromeritics AutoChem II 2920 Chemisorption analyzer and an Agilent 5973N mass-selective detection (MSD) system to identify the gaseous products evolved from zeolite samples. Methods to titrate protons at Al heteroatoms ($H_{\rm Al}^+$) in B–Al–MFI zeolites have been reported by Kester et al. In short, NH₄-form B–Al–MFI samples (0.04–0.06 g, sieved to 180–250 μ m) were supported between two quartz wool plugs in a U-shaped quartz cell and placed in a clam-shell furnace. Samples were then heated under flowing He (15 cm³ s⁻¹ g_{cat}⁻¹, UHP, 99.999%, Indiana Oxygen) to 433 K (0.167 K s⁻¹) and held isothermally for 4 h to remove NH₃ bound to B heteroatoms. The temperature was then increased to 873 K (0.167 K s⁻¹) and evolved gases were sent to the MSD for quantification. Calibration and deconvolution methods were performed

according to previous reports. ²⁸ Methods previously reported to titrate residual protons on partially metal-exchanged zeolites were used here to measure residual protons on Co–B–Al–MFI. ²⁸ The Co-forms of B–Al–MFI samples (0.04–0.06 g, sieved to 180–250 μ m) were heated under flowing dry air (15 cm³ s⁻¹ g_{cat}⁻¹, 99.999% UHP, Indiana Oxygen) to 673 K, held for 2 h, then cooled to 433 K, at which point gas-phase NH₃ was introduced for 4 h. A subsequent wet He purge at 433 K was used to purge NH₃ adsorbed at at all sites except Brønsted sites associated with framework Al, prior to TPD.

UV–visible spectroscopy was used to determine the oxidation state of Co ions and to detect the presence of Co-oxides on zeolite samples following exchange with $\text{Co}(\text{NO}_3)_2$ solutions. Diffuse reflectance UV–vis (DRUV–vis) spectra were recorded under in situ conditions using a Varian Cary 5000 UV–vis–NIR Spectrophotometer attached with a Harrick Scientific Praying Mantis diffuse reflectance accessory. Baseline spectra were recorded for every sample using poly(tetrafluoroethylene) (PTFE, 1 μ m powder, Sigma–Aldrich) as the 100% reflectance standard, and then converted to an absorption spectrum using the Kubelka–Munk (F(R)) function. Spectra were recorded from 12 500 to 50 000 cm⁻¹ at a scan rate of 167 cm⁻¹ s⁻¹ at 673 K.

Crystallites were imaged using scanning electron microscopy (SEM) using an FEI Quanta 3D FEG Dual-beam SEM system. Prior to imaging, samples were coated with platinum to reduce charging. Images were taken at 5000× to 15 000× magnification with an accelerating voltage of 15 kV and spot size of 6 μ m.

The amount of TPA^+ and EDA organic SDAs occluded in solid zeolite products was estimated from the C and N elemental compositions of as-synthesized zeolites measured with CHN analysis (Galbraith Laboratories, PerkinElmer 2400 Series II CHNS/O Analyzer).

Thermogravimetric analysis (TGA) experiments were performed on as-synthesized B–Al–MFI–TPA zeolites using a TA Instruments SDT Q600 thermogravimetric analyzer and differential scanning calorimeter (TGA-DSC) by heating 0.02 g of as-synthesized B–Al–MFI in flowing dry air (83.3 cm³ s $^{-1}$ g_{cat} $^{-1}$, UHP, 99.999%, Indiana Oxygen) to 523 K (0.167 K s $^{-1}$) and holding for 0.5 h to remove physisorbed water before further heating to 1073 K (0.167 K s $^{-1}$).

2.4. Measurement of Methanol Dehydration Kinetics. Detailed experimental methods and calculations for first- and zero-order rate constants for methanol dehydration are reported in our prior publications;²⁹ here, we provide an abridged summary. Methanol dehydration rates were measured in a tubular quartz reactor (7 mm inner diameter) with a packed bed supported by quartz wool plugs. All rates were measured under differential conversions (<15%) at 415 K. Temperatures were measured by Type K thermocouple placed on the external surface of the quartz reactor aligned with the center of the catalyst bed and the temperature was controlled with resistively heated, three-zone furnaces (Applied Test Systems Series 3210) and Watlow controllers (EZ-Zone series). In a typical experiment, 0.02-0.03 g of H-B-Al-MFI were pelleted and sieved to retain particles 180–250 μm in diameter and treated in 5% O₂ with balance He (50 cm³ s⁻¹ g_{cat}^{-1} , 99.999%, Indiana Oxygen) to 773 K (0.033 K s⁻¹) for 4 h before cooling to reaction temperature under flowing He (200 cm³ s⁻¹ g_{cat}⁻¹, UHP 99.999%, Indiana Oxygen). Methanol (99 wt %, Sigma-Aldrich) was introduced via syringe pump (Legato 100, KD Scientific) into flowing He at

Table 1. Elemental Composition of B-Al-MFI Zeolites of Varying Al and B Content

B-Al-MFI-SDA (Si/B, Si/Al)	$\mathrm{Si/Al}_{\mathrm{gel}}$	Si/Al _{tot} ^a	$\mathrm{Si/B}_{\mathrm{gel}}$	Si/B _{tot} ^b	$Si/(Al+B)_{tot}$	$\mathrm{H^{+}_{Al}/Al_{tot}}^{c}$
B-Al-MFI-TPA (2.5, 50)	50	59	2.5	48	26.4	0.84
B-Al-MFI-TPA (10, 50)	50	57	10			0.98
B-Al-MFI-TPA (25, 50)	50	66	25	120	43.2	0.98
B-Al-MFI-TPA (50, 50)	50	54	50			1.03
B-Al-MFI-TPA (100, 50)	50	51	100			0.95
B-Al-MFI-TPA (200, 50)	50	69	200	340	57.4	1.09
B-Al-MFI-TPA (500, 50)	50	42	500			0.81
B-Al-MFI-TPA (B-free, 50)	50	52	∞ (B-free)	∞ (B-free)	52	0.96
B-Al-MFI-EDA (2.5, 50)	50	53	2.5	26	17.3	1.02
B-Al-MFI-EDA (10, 50)	50	58	10			1.09
B-Al-MFI-EDA (25, 50)	50	51	25	39	22.2	0.95
B-Al-MFI-EDA (50, 50)	50	60	50			1.08
B-Al-MFI-EDA (200, 50)	50	58	200	240	46.5	
B-Al-MFI-EDA (500, 50)	50	53	500			0.78
B-Al-MFI-EDA (B-free, 50)	50	58	∞ (B-free)	∞ (B-free)	58	0.92
B-MFI-EDA	∞ (Al-free)	∞ (Al−free)	2.6	30.0		

^aDetermined by AAS. Errors are ±10%. ^bDetermined by ICP-OES. Errors are ±10%. ^cDetermined by NH₃ TPD. Errors are ±15%.

varying flow rates to change the partial pressure. Partial pressures were measured in a reactor bypass, and all reactant and product concentrations were measured via a gas chromatograph equipped with a flame ionization detector (HP Plot-Q KCl column, 0.53 mm inner diameter (ID) \times 30 m \times 40 μ m film, Agilent). Dimethyl ether and water were the only products observed on all catalysts tested under all conditions. Methane (25% CH₄ in argon, 99.999%, Indiana Oxygen) was used as an internal standard, and introduced into the reactor effluent stream (0.83 cm³ s⁻¹).

3. RESULTS AND DISCUSSION

3.1. Synthesis of B–Al–MFI Zeolites and Structural Characterization. B–Al–MFI samples with varying Si/B and Si/Al ratios were synthesized by two different methods, one using tetra-*n*-propylammonium (TPA⁺) as the only organic SDA (denoted B–Al–MFI–TPA) and the other using both TPA⁺ and ethylenediamine (EDA) as organic SDAs (denoted B–Al–MFI–EDA). Powder XRD patterns of all B–Al–MFI samples were consistent with the MFI topology (Figures S1–S3).²⁷ Micropore volumes calculated from N₂ adsorption isotherms (0.13–0.15 cm³ g⁻¹, Figures S4 and S5) were also consistent with the MFI topology for all samples. The elemental compositions of synthesis solutions and crystalline solids are summarized in Table 1.

The coordination of Al and B heteroatoms in MFI frameworks was probed using 27 Al MAS NMR (Figure S6) and 11 B MAS NMR (Figure S7). 27 Al MAS NMR spectra of all samples showed a resonance centered at 53 ppm for tetrahedrally coordinated framework Al^{26,30} and a small feature at 0 ppm for octahedrally coordinated extraframework Al. These features were used to estimate the fraction of Al incorporated into framework positions, which was close to unity for all samples ($Al_f/Al_{tot} = 0.90-0.98$, Table S1). ¹¹B MAS NMR spectra of all samples showed a resonance centered at -3 ppm for tetrahedrally coordinated boron,³¹ and only minor features for trigonal B at ~15 ppm in some B-Al-MFI-TPA samples. This suggests that B heteroatoms are predominantly tetrahedrally coordinated under hydrated conditions at ambient temperature in the B-Al-MFI samples studied here. Tetrahedral B in B-MFI can be partially removed from the framework to form trigonal B species

through a series of reversible hydrolysis reactions of B–O–Si bonds upon dehydration, ^{31,32} and features in ¹¹B MAS NMR at –3 ppm for tetrahedral B can persist when B has less than four framework bonds, often from hydroxide or water ligands bound during hydration. Given the hydrated conditions used in ¹¹B MAS NMR experiments, we cannot comment further on the number of B–O–Si bonds retained in B–Al–MFI zeolites after oxidative treatments and aqueous-phase ion-exchange procedures.

Although both tetrahedral Al and B heteroatoms can be charge-compensated by Brønsted acid protons in zeolite frameworks, protons associated with framework Al are stronger acids than those associated with B, as reflected in deprotonation energies (DPE) that are ~70 kJ mol⁻¹ lower for protons at Al than at B. 25 Therefore, rigorous normalization of acid-catalyzed turnover rates in boroaluminosilicates requires discrimination between Brønsted acidic OH groups associated with Al and B heteroatoms, even when the quantity of B heteroatoms is much greater than Al (Al/B < 0.01), because observed catalytic reactivity originates predominantly from protons at framework Al (e.g., n-hexane cracking).2-Temperature-programmed desorption (TPD) of NH₃ from B-Al-MFI following saturation in aqueous-phase NH₄NO₃ solution overestimates the number of framework Al heteroatoms, ²² because NH₃ also binds to trigonal and tetrahedral B heteroatoms³³ and thus the NH₃ evolved during TPD may originate from B or Al heteroatoms. NH3 titrants can be used to quantify the number protons at framework Al heteroatoms (H⁺_{Al}) in B–Al–MFI zeolites either by saturation of B and Al sites with NH₄⁺ by aqueous-phase ion-exchange and selective removal of NH₃ from B via purging in flowing dry He (433 K), or by saturation in gaseous NH3 at temperatures that result in selective adsorption at $H^{^{+}}_{\ Al}$ sites (433 K). 22 These procedures were used to quantify H+Al in the suite of B-Al-MFI zeolites synthesized here, and the results are summarized in Table 1. These values agree quantitatively with the total amount of Al measured by atomic absorption spectroscopy $(H_{Al}^+/Al_{tot} =$ 0.78-1.09) in all B-Al-MFI samples (Figure 1), consistent with the predominant incorporation of Al into framework positions as evidenced by ²⁷Al MAS NMR. Only negligible NH₃ (<0.01 mmol g⁻¹) is evolved from B-MFI-EDA samples

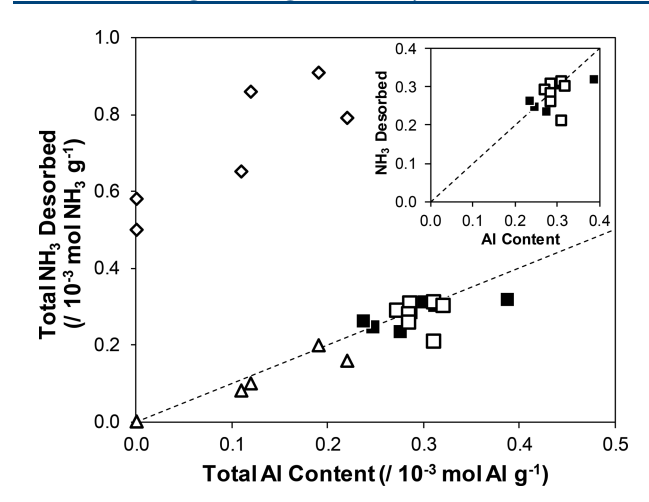


Figure 1. NH₃ desorbed during TPD from B–Al–MFI–TPA (open squares) and B–Al–MFI–EDA (closed squares) samples after aqueous-phase NH₄NO₃ saturation and subsequent helium purge; NH₃ desorbed from B–Al–MFI–EDA zeolites²² after aqueous-phase NH₄NO₃ saturation with (open triangles, reported by Kester et al.)²² and without (open diamonds, reported by Kester et al.)²² purging in He at 433 K. The inset shows selective titration data for a clear visual description. Dashed line represents parity. Adapted with permission from ref 22. Copyright 2018 American Chemical Society.

in these procedures because ammonia associated with B heteroatoms do not remain adsorbed at 443 K.

Representative SEM images of B–Al–MFI–EDA samples are shown in Figure 2. Images shown in Figure 2a–d correspond to B–Al–MFI–EDA samples made from synthesis gels with relatively low B content (Si/B = 25) and varying Al content (Si/Al = 50, 150, 300, 500), and those shown in Figure 2e–h were made with synthesis gels with higher B content (Si/B = 2.5) and varying Al content (Si/Al = 50, 150, 300, 500). Elemental composition of the crystalline solids, mean crystallite lengths, and diffusion parameters of these samples

are given in Table 2. Crystallite size distributions obtained by measuring at least 250 particles per sample (Figure S8) are

Table 2. Mean Crystallite Lengths and Diffusion Parameters for B–Al–MFI–EDA Samples Crystallized from Synthesis Gels Containing Low (Si/B_{gel} = 25) and High (Si/B_{gel} = 2.5) B Content

sample name	Si/ Al ^a	mean crystallite length $(L)^b$ (μ m)	diffusion parameter (Ψ) $(/10^{-6} \text{ mol H}^+_{Al} \text{ nm}^{-1})$
B-Al-MFI- EDA (25, 50)	51	12.6 ± 1.7	42
B-Al-MFI- EDA (25, 150)	184	13.2 ± 0.9	13
B-Al-MFI- EDA (25, 300)	229	14.1 ± 1.0	12
B-Al-MFI- EDA (25, 500)	494	15.2 ± 0.8	6
B-Al-MFI- EDA (2.5, 50)	53	1.3 ± 0.3	0.4
B-Al-MFI- EDA (2.5, 150)	181	1.6 ± 0.3	0.2
B-Al-MFI- EDA (2.5, 300)	303	1.9 ± 0.5	0.2
B-Al-MFI- EDA (2.5, 500)	466	2.6 ± 0.5	0.2

"Determined by AAS. Determined from analyzing >250 particles per sample imaged by SEM; uncertainty given as the standard deviation in crystallite size distribution.

unimodal and symmetric. Among samples of fixed Si/B ratio in the synthesis solution (either 2.5 or 25), mean crystallite sizes are similar (within 1.5-fold) with varying Al content (Table 2). In contrast, among samples of similar Si/Al ratio (Si/Al of either 50, 150, 300, or 500), mean crystallite sizes increased with decreasing B content by a larger factor of \sim 10 (Table 2). Crystallites synthesized from solutions containing Si/B = 25 are coffin-shaped (Figure 2a–d), while those from solutions with Si/B = 2.5 are rod-shaped and often aggregated into small

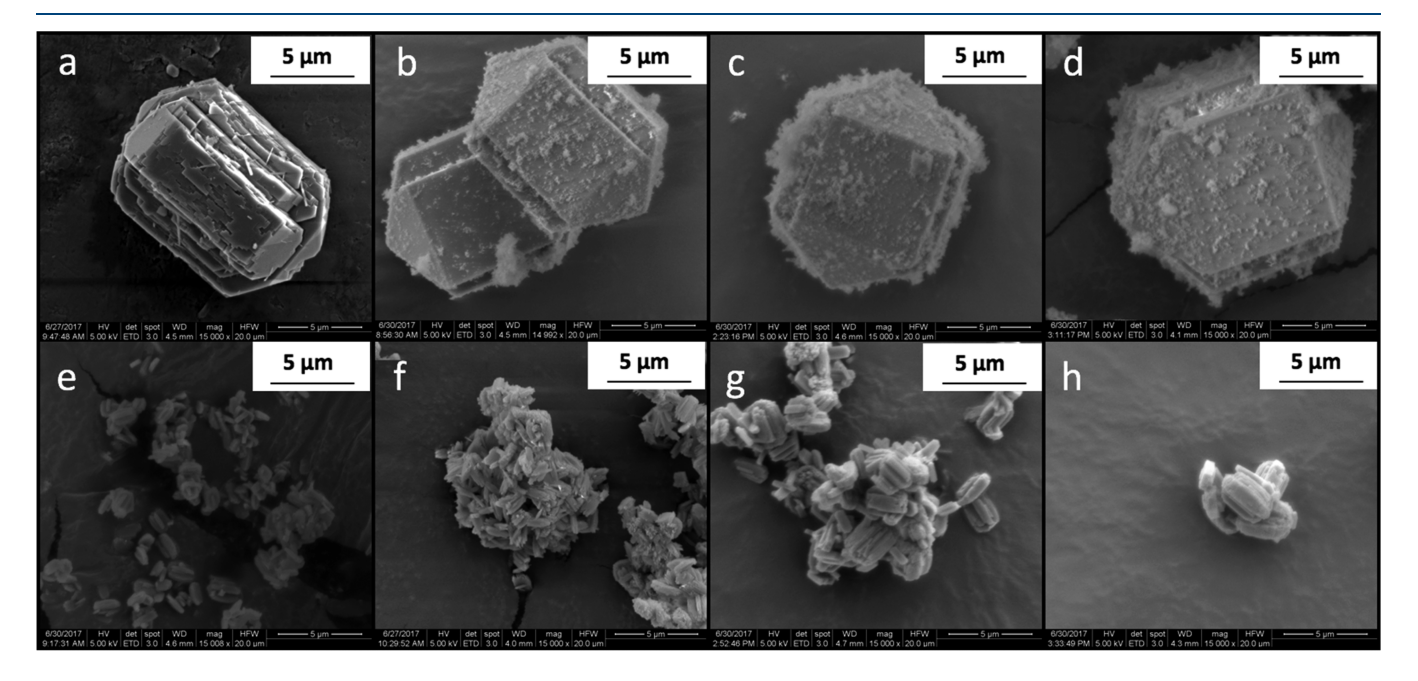


Figure 2. SEM micrographs of MFI zeolite samples: (a) B-Al-MFI-EDA (25, 50), (b) B-Al-MFI-EDA (25, 150), (c) B-Al-MFI-EDA (25, 300), (d) B-Al-MFI-EDA (25, 500), (e) B-Al-MFI-EDA (2.5, 50), (f) B-Al-MFI-EDA (2.5, 150), (g) B-Al-MFI-EDA (2.5, 300), and (h) B-Al-MFI-EDA (2.5, 500).

clusters (Figure 2e-h). These findings are consistent with previous reports of B-Al-MFI zeolites made with similar synthetic protocols,²² where it was hypothesized that ethylenediamine acts as both a structure directing agent during B-Al-MFI synthesis and as a ZGM by binding to MFI crystal facets during synthesis to influence anisotropic crystal growth. 18,19 Similar observations describe changes in the morphology of B-Al-MFI-TPA samples crystallized from synthesis solutions of fixed Si/Al ratio (50) and decreasing B content (Si/B = 2.5-500, Figure S9). These findings are similar to those for Al-MFI with increasing Al content, 13,34 indicating that it may be plausible that the smaller crystallites in B-Al-MFI-EDA zeolites with increasing B content are not solely due to the binding of EDA to external crystallite surfaces during growth. These results collectively indicate that B-Al-MFI crystallite sizes are predominantly influenced by the Si/B ratios present in synthesis solutions for the conditions studied here, when using either TPA+ only or EDA/TPA+ mixtures as the organic SDAs.

3.2. Validation of Co2+ Exchange Methods to Quantify Proximal Al Sites in MFI Zeolites. The use of Co²⁺ cations as titrants to quantify proximal (or "paired") AlO_{4/2} ensembles in zeolite frameworks requires methods to verify that saturation Co2+-exchange capacities have been attained and that cation site balances satisfy the expected stoichiometry of two monovalent cations (e.g., H⁺ or Na⁺) replaced per divalent Co²⁺ cation, as well as spectroscopic evidence of the presence of Co²⁺ species and the absence of other phases (e.g., Co-oxides). A variety of conditions have been reported in the literature for Co2+ ion exchange to titrate proximal Al sites in MFI zeolites. Dědeček and co-workers have reported using different Co²⁺ precursors, concentrations (0.0002-0.1 M), number of sequential exchanges, and temperatures (298–350 K) to saturate Na-form MFI zeolites with $\mathrm{Co^{2+}}$ cations. ^{35,36} Bell and co-workers report using 0.05 M Co(NO₃)₂ solutions in a single exchange for 24 h on Na-form samples,³⁷ and Corma and co-workers report using three sequential exchanges using a 0.05 M Co(NO₃)₂ solution at room temperature for 8 h.38 Given the diverse range of Co2+ ion-exchange procedures reported previously for MFI zeolites, we first determined the conditions required for Co²⁺ saturation of Na-form Al-MFI zeolites by performing experiments with varying Co(NO₃)₂ concentrations in solution, duration of each exchange, temperature, and number of sequential repetitions with fresh $Co(NO_3)_2$ solutions.

A commercially available Al-MFI zeolite sample (Zeolyst CBV2314, Si/Al = 11.5) was used for validation of Co^{2+} saturation protocols. At 293 K, the amount of Co²⁺ exchanged onto this Na-form MFI sample increased at low concentrations and reached a constant value of 2 \times Co²⁺/Al_{tot} \sim 0.14 for Co(NO₃)₂ concentrations above 0.05 M (Figure 3). Additionally, the amount of ion-exchanged Co2+ did not vary systematically with durations longer than 20 h in 0.25 M Co(NO₃)₂ solutions (Figure S10), suggesting that Na-MFI samples were saturated after 20 h of exposure to 0.25 M Co(NO₃)₂ solutions at 293 K. However, upon repeating exchange protocols up to eight times with fresh Co(NO₃)₂ solutions (0.25 or 0.50 M) after washing and drying samples between repetitions, the amount of Co2+ exchanged onto the solid increased systematically and approached an asymptotic value of $2 \times \text{Co}^{2+}/\text{Al}_{\text{tot}} \sim 0.30$ (Figure 3). These systematic trends were independent of the concentration of $\text{Co(NO}_3)_2$ solution (0.25 or 0.5 M) (Figure 3) and a 2:1 exchange of Na⁺

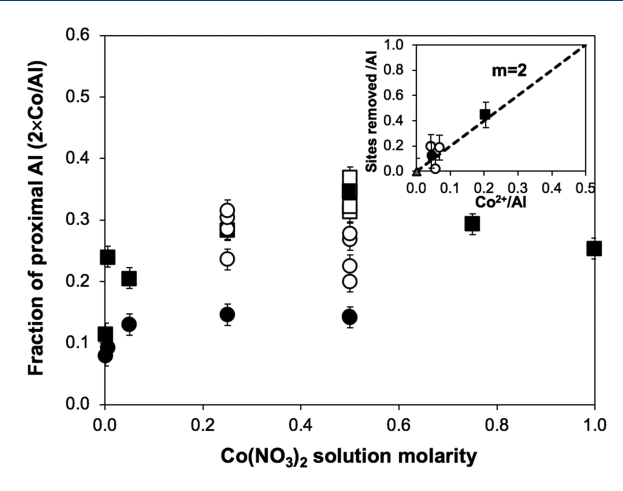


Figure 3. Aqueous-phase $\mathrm{Co^{2^+}}$ ion exchange capacity of Al–MFI (Zeolyst CBV2314, Si/Al = 11.5) with $\mathrm{Co(NO_3)_2}$ solutions (0.001–1.0 M) for 24 h at 293 K (circles) and 353 K (squares). Single (closed) and multiple repetitions (open, 2–8 replicate exchanges). Inset shows the site balances of divalent $\mathrm{Co^{2^+}}$ and residual monovalent (H⁺ and Na⁺) cations compared to the Na-form (triangle). The dashed line corresponds to of the removal of two monovalent cations with each divalent $\mathrm{Co^{2^+}}$ ion.

or H^+ for Co^{2+} was confirmed with NH_3 TPD (Figure 3 inset), indicating that single repetitions of Co^{2+} ion-exchange procedures at 293 K did not saturate all proximal Al sites with Co^{2+} cations.

Next, we equilibrated Na-form Al-MFI with aqueous Co(NO₃)₂ solutions at 353 K for 24 h. The number of Co²⁺ ions increased with Co(NO₃)₂ concentration following Langmuirian-type behavior with saturation $2 \times \text{Co}^{2+}/\text{Al}_{\text{tot}}$ values of ~0.30 reached by 0.25 M (Figure 3) after a single ion exchange. Additional repetitions using 0.25 and 0.50 M Co(NO₃)₂ solutions at 353 K did not increase the amount of Co²⁺ retained (Figure 3). DRUV-vis spectra collected at 673 K for dehydrated Co-MFI zeolites with varying Co²⁺ content $(2 \times \text{Co/Al}_{\text{tot}} = 0.12-0.30)$ show features for the d-d transition of bare Co2+ ions bound to lattice O atoms $(15,100-22,000 \text{ cm}^{-1}, \text{ Figure S11})^{.35}$ Absorption bands in the region reflecting charge transfer transitions in Co-oxides (around 30 000 cm⁻¹)³⁹ do not appear in the spectra of any Co-MFI samples (Figure S12), indicating the higher Co content resulting from higher temperature ion-exchange conditions were not a result of oxide formation.

The closure of cation exchange site balances between Co-Na-exchanged Al–MFI samples and the parent H–Al–MFI sample was verified by temperature-programmed desorption of NH₃ from Brønsted acidic protons in Al–MFI. The quantification of residual H⁺ and Na⁺ on Co–Na-exchanged Al–MFI samples, when compared to the number of H⁺ sites on the parent H–Al–MFI sample, are shown in the inset of Figure 3. Al–MFI samples that were exchanged at both 298 and 353 K showed agreement with stoichiometry expected (parity line in Figure 3) for each Co²⁺ cation replacing two Na⁺ or H⁺ sites. These results indicate that Co²⁺ can be used to quantify proximal Al arrangements within MFI zeolites, upon verifying that Co ion-exchange protocols indeed lead to saturation of all exchange sites with Co²⁺.

3.3. Effect of Structure-Directing Agents on Al Distribution of B-Al-MFI Zeolites. Using the ion-exchange methods described in section 3.2, B-Al-MFI-TPA and B-Al-MFI-EDA zeolites were saturated with Co²⁺

cations in aqueous solution (0.5 M Co(NO₃)₂ solution at 353 K for 24 h). B–Al–MFI–TPA samples contain 20–40% Al in proximal configurations (2 × Co²⁺/Al_{tot} = 0.20–0.40), and no systematic trend in the fraction of proximal Al was observed with increasing B content in the synthesis solution (Figure 4).

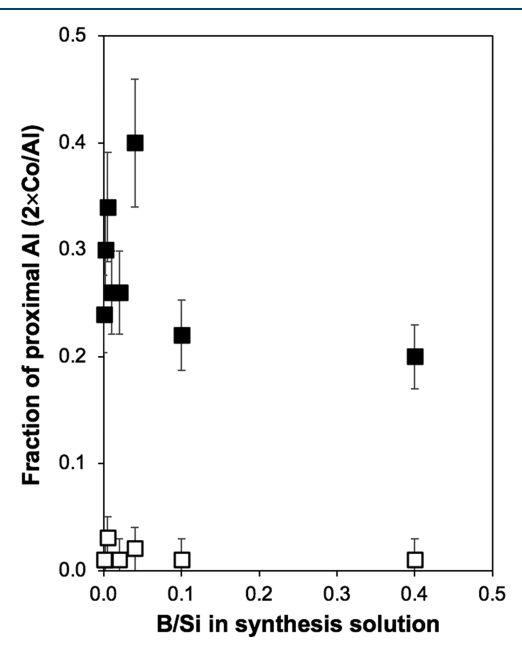


Figure 4. Fraction of Al in proximal configurations measured by Co^{2+} titration (353 K, 24 h, 0.5 M $Co(NO_3)_2$), for a suite of B–Al–MFI samples of similar Al composition (Si/Al \sim 50) prepared using two different synthesis methods (B–Al–MFI–TPA (closed), B–Al–MFI–EDA (open)) as a function of the B/Si ratio in the synthesis solution

Absorption bands in the region reflecting charge transfer transitions in Co-oxides (ca. 30 000 cm⁻¹)³⁹ do not appear in the spectra of Co²⁺-exchanged B-Al-MFI-TPA samples, as expected for samples saturated with Co²⁺ ions (Figure S13). In contrast, B-Al-MFI-EDA samples of similar bulk composition contain >95% of their framework Al present as isolated sites across a range of Si/B ratios (Figure 4). The use of $Al(OH)_3$ instead of $Al(NO_3)_3$ as the Al precursor did not affect the number of proximal Al in B-Al-MFI-EDA zeolites (Table S2), however, using colloidal silica instead of fumed silica in B-Al-MFI-TPA (25, 50) zeolites decreased the percentage of Al in proximal configurations from 40 to 16% (Table S2). Different Al and Si precursors have also been reported to influence the fraction of Al in proximal configurations in MFI⁴⁰ and CHA²⁹ zeolites, and the specific Al and Si precursors used in synthetic solutions may affect framework Al arrangements in B-Al-MFI zeolites in ways that are not currently well-understood.

Among the samples in this study, we note that the most significant difference in the percentage of Al in proximal configurations is observed between zeolites made with TPA+ only (finite values, in the range of 16–40%) or EDA/TPA+ mixtures (essentially zero values, < 5%). Therefore, differences in Co²⁺ saturation values between B–Al–MFI–TPA and B–Al–MFI–EDA samples appear to reflect the influence of TPA+ and EDA/TPA+ mixtures on the relative proximity of framework Al heteroatoms. The amounts of EDA and TPA molecules occluded within B–Al–MFI crystallites were determined using carbon–hydrogen–nitrogen (CHN) ele-

mental analysis to estimate the fraction of this organic content comprising either TPA $^+$ (C/N = 12) or EDA (C/N = 1). Among B-Al-MFI-TPA samples, approximately four TPA $^+$ molecules were occluded per MFI unit cell (3.7–3.9 TPA $^+$ per unit cell, Table 3, Figure 5), corresponding to one TPA $^+$

Table 3. Quantities of Occluded TPA⁺ and Co²⁺ Ion Exchange Capacity in B-Al-MFI-TPA Zeolites

B-Al-MFI-SDA (Si/B, Si/Al)	C/N ^a	$\begin{array}{c} TPA \\ (/mmol \ g^{-1}) \end{array}$	TPA/Al _{tot}	$2 \times \text{Co/Al}_{\text{tot}}^{\ \ b}$
B-Al-MFI-TPA (2.5, 50)	11.0	0.68	2.48	0.20
B-Al-MFI-TPA (10, 50)	11.2	0.54	1.86	0.22
B-Al-MFI-TPA (25, 50)	11.5	0.54	2.26	0.40
B-Al-MFI-TPA (50, 50)	11.8	0.66	2.19	0.26
B-Al-MFI-TPA (100, 50)	11.3	0.66	2.08	0.26
B-Al-MFI-TPA (200, 50)	11.5	0.65	2.41	0.34
B-Al-MFI-TPA (500, 50)	10.9	0.67	1.75	0.30
B-Al-MFI-TPA (B-free, 50)	11.3	0.63	2.00	0.24

^aDetermined by CHN elemental analysis. Errors are ±10%. ^bDetermined by AAS. Errors are ±15%.

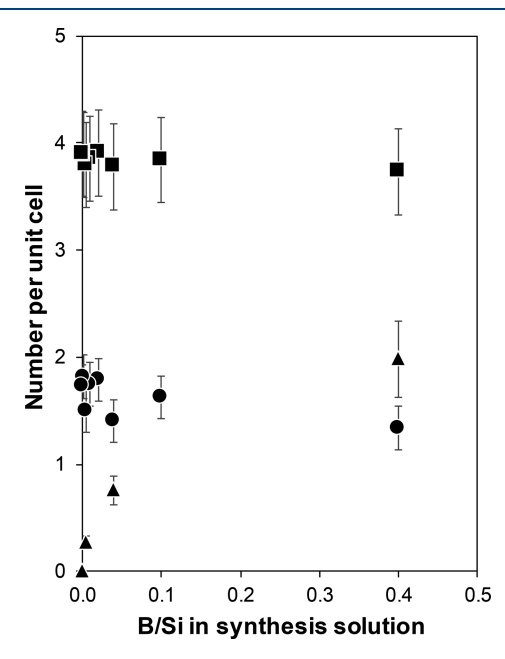


Figure 5. Number of TPA^+ molecules (squares), Al heteroatoms (circles), and B heteroatoms (triangles) incorporated into B-Al-MFI-TPA zeolites.

molecule per channel intersection in the MFI topology, ⁴¹ independent of the B content in the synthesis solution. Organic contents measured by thermogravimetric analysis (TGA) showed a loss of \sim 12 wt % in B–Al–MFI–TPA samples, consistent with \sim 4 TPA⁺ molecules per MFI unit cell. C/N ratios of occluded organics in these samples ranged from 10.9–11.8 (Table 3), close to the expected ratio of 12 for TPA⁺. Framework Al contents were similar among these samples (1.3–1.8 Al_f per unit cell, Figure 5) and close to that expected for nearly complete Al incorporation from synthesis

solutions (~1.9 Al_f per unit cell) into crystalline products. Only a fraction of the B from synthesis solutions was incorporated into the solid B-Al-MFI-TPA crystallites (Figure 5), consistent with previous reports on the partial incorporation of B into MFI zeolites from synthesis solutions containing TPA⁺.23,42,43 Boric acid (B(OH)₃) precursors equilibrate with borate (B(OH)₄⁻) in aqueous media, and borate species are predominant under the basic conditions used in hydrothermal synthesis (pH >11). Unlike Al(OH)₄ species that condense with Si precursors to form Al-O-Si bonds, borate species are unable to undergo nucleophilic S_N2type attack by Si(OH)₄ groups to form B-O-Si bonds, because B cannot adopt the pentacoordinate transition state required for this condensation reaction. 16 Hydrophobic domains near alkyl groups in TPA+ molecules are proposed to decrease the local concentration of water and hydroxide ligands with free lone pairs around clathrated TPA+ molecules,⁴⁴ thereby shifting equilibrium toward boric acid that can undergo S_N 2-type reactions with Si precursors to incorporate B. ¹⁶ The maximum amount of B and Al incorporated in B-Al-MFI-TPA (3.3 per unit cell) is similar to the TPA+ content (3.7 per unit cell), consistent with the charge-compensation of a single framework heteroatom per TPA+ cation (Figure 6). Therefore, we surmise that B

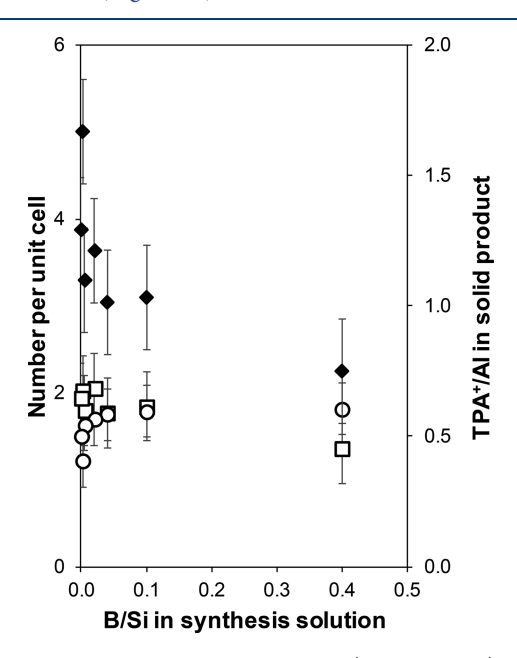


Figure 6. Number of TPA^+ molecules (open squares) and Al heteroatoms (open circles) incorporated into B-Al-MFI-EDA zeolites. Ratio of TPA^+/Al (closed diamonds) is given on the secondary axis.

incorporation in B–Al–MFI–TPA zeolites is limited by the equilibrium between boric acid and borate, where boric acid is likely associated with TPA⁺ during hydrothermal synthesis, and by the inability for TPA⁺ to charge-compensate more than one framework heteroatom per MFI intersection.

Al-MFI zeolites that do not contain boron and are synthesized from solutions containing TPA+ as the sole SDA contain framework Al sited in proximal locations that can charge-compensate for Co²⁺, and the addition of B to such synthesis solutions does not systematically affect the population of proximal Al sites in the resulting crystalline products (Figure 4). This finding is consistent with previous Al-MFI syntheses using TPA⁺ as the only SDA that contain proximal Al that compensate Co²⁺ cations. 40 Therefore, a fraction of framework Al heteroatoms sited by TPA+ cations occluded in adjacent MFI channel intersections must be close enough to charge-compensate Co2+ cations. In the case of B-Al-MFI-TPA zeolites with Si/Al ~ 50, approximately half of these TPA+ cations charge-compensate Al heteroatoms in the lattice, giving rise to adjacent intersections that contain TPA+- $AlO_{4/2}$ ion pairs. The presence of framework B heteroatoms does not affect Co²⁺ saturation values because B heteroatoms likely do not have four framework bonds under the acidic conditions (pH ~5) used in Co²⁺ ion-exchange.⁴⁵

Among B–Al–MFI–EDA samples, molar C/N ratios were lower (C/N = 2.3–4.8) than in B–Al–MFI–TPA samples and decreased with increasing B content in the synthesis solution (Table 4), reflecting the incorporation of EDA (C/N = 1) into crystalline products. Equation 2 was used to calculate the occluded EDA/TPA ratio in B–Al–MFI–EDA samples (Table 4), assuming that both TPA $^+$ and EDA remain intact during hydrothermal synthesis.

$$\frac{\text{EDA}}{\text{TPA}} = \frac{12 - \frac{\text{C}}{\text{N}}}{2\left(\frac{\text{C}}{\text{N}} - 1\right)} \tag{2}$$

Only ~2 TPA⁺ molecules are occluded per unit cell in B–Al–MFI–EDA zeolites (Figure 6), which is approximately half of that occluded per unit cell in B–Al–MFI–TPA zeolites, likely a result of the TPA⁺/Si ratio of 0.02 (corresponding to ~2 TPA⁺ per unit cell) that was used in synthesis solutions to crystallize B–Al–MFI–EDA zeolites. These results resemble those for MFI zeolites made from TPA⁺–Na⁺ mixtures with TPA⁺/Si ratios⁴⁶ similar to those reported here. TPA⁺/Al ratios are ~1 in B–Al–MFI–EDA zeolites (Figure 6), independent of B content, again reflecting the molar composition of the synthesis solution. In the absence of B, approximately 2 EDA molecules are occluded per unit cell in Al–MFI–EDA zeolites (Figure 7). Therefore, we conclude that EDA can also act as an SDA for the MFI framework⁴⁵

Table 4. Quantities of Occluded Organic SDAs and Co²⁺ Ion Exchange Capacity in B-Al-MFI-EDA Zeolites

B-Al-MFI-SDA (Si/B, Si/Al)	C/N ^a	EDA/TPA	TPA $(/mmol g^{-1})$	EDA $(/mmol g^{-1})$	TPA/Al _{tot}	$2 \times \text{Co/Al}_{\text{tot}}^{\ \ b}$
B-Al-MFI-EDA (2.5, 50)	2.3	3.8	0.21	0.80	0.74	0.01
B-Al-MFI-EDA (10, 50)	2.9	2.4	0.27	0.64	0.87	0.01
B-Al-MFI-EDA (25, 50)	3.3	1.9	0.30	0.55	0.94	0.02
B-Al-MFI-EDA (50, 50)	4.2	1.2	0.37	0.45	1.1	0.01
B-Al-MFI-EDA (200, 50)	4.2	1.2	0.37	0.45	1.3	0.03
B-Al-MFI-EDA (500, 50)	4.8	1.0	0.38	0.36	1.2	0.01
B-Al-MFI-EDA (B-free, 50)	4.2	1.2	0.31	0.39	0.91	0.01

^aDetermined by CHN elemental analysis. Errors are ±10%. ^bDetermined by AAS. Errors are ±15%.

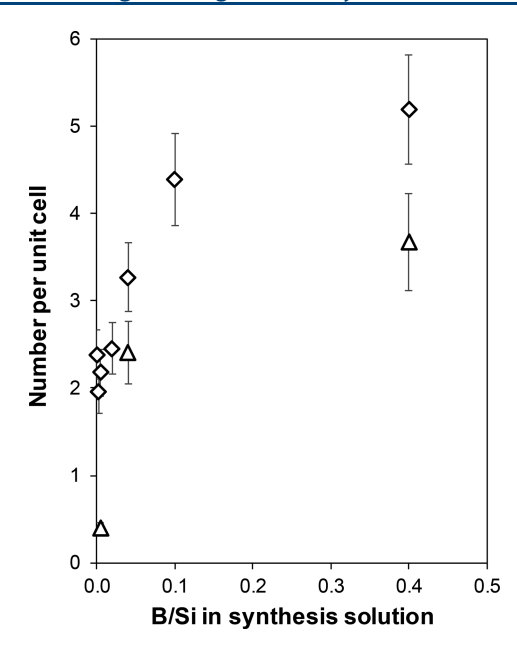


Figure 7. Number of EDA molecules (open diamonds) and B heteroatoms (open triangles) retained in B-Al-MFI-EDA zeolites as a function of B/Si in the synthesis solution.

when Si/TPA+ ratios in synthesis solutions are greater than 24, and not all silicate precursors can exchange with water contained in TPA+-clathrate structures. 15 We surmise that TPA⁺ cations are responsible for siting Al in B-Al-MFI-EDA zeolites, given their near-stoichiometric presence in all samples. With increasing B/Si in synthesis mixtures, a slight decrease in the amount of TPA+ retained on the solid to 1.4 per unit cell is observed, while EDA contents increase systematically to 5.2 per unit cell. B retained in the solid product increases in parallel with EDA, up to 3.7 per unit cell (Figure 7), and more B is retained in B-Al-MFI-EDA than in B-Al-MFI-TPA zeolites (Figure 6) for a given B/Si ratio used in the synthesis solutions. Similar observations of TPA+ exclusion have been reported for B-MFI zeolites made with TPA+ and alkali metal cations (e.g., K⁺, Cs⁺), where these cations replace some TPA⁺ and enable incorporating more than 4 B heteroatoms per MFI unit cell. 47 The amount of EDA retained in the crystalline products increases with the B content in the solid (Figure 8) with a ratio of approximately two B heteroatoms per EDA molecule, consistent with EDA-boric acid complexes containing two B atoms that have previously been shown to behave as structure directing agents for B-MFI zeolites. 20,21

The presence of predominantly isolated Al heteroatoms in B-Al-MFI-EDA zeolites contrasts the 20-40% Al in proximal configurations found in B-Al-MFI-TPA zeolites of similar bulk composition. Given that approximately half of MFI intersections are occupied by TPA+ in B-Al-MFI-EDA zeolites, the number of adjacent intersections containing TPA+ is lower, on average, than that in B-Al-MFI-TPA zeolites. Therefore, we surmise that the presence of predominantly isolated Al in B-Al-MFI-EDA zeolites is a consequence of the dilution of TPA+ occupancy of intracrystalline void spaces in the crystalline solids by co-occluded EDA, which does not appear to site Al heteroatoms under the conditions studied. This finding provides a link between the fractional occlusion of TPA^+ within MFI frameworks (~1.5 per unit cell) and the resulting isolation of framework Al. In this case, EDA is occluded within void spaces not occupied by TPA+ in Al-

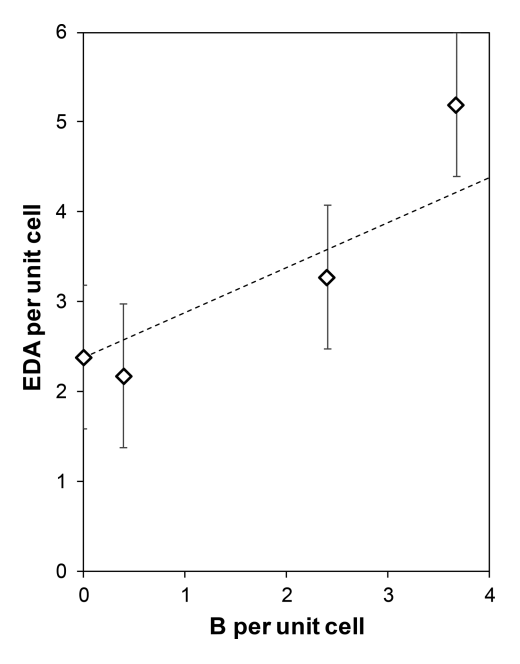


Figure 8. Number of EDA molecules retained in B-Al-MFI-EDA zeolites as a function of B content. Dashed line denotes a slope of 0.5 (corresponding to a B/EDA stoichiometry of 2).

MFI–EDA zeolites, and the addition of B to synthesis solutions forms B–EDA complexes that exclude some TPA⁺ molecules and concurrently incorporate approximately two B heteroatoms per EDA into the MFI framework. These conclusions highlight the roles of TPA⁺ and EDA SDAs on the siting and prevalence of Al and B heteroatoms in MFI zeolites by relating the compositions of the synthesis solutions to those of crystalline products.

3.4. Probing Al Location in Different Void Environments of B-Al-MFI Zeolites via Kinetics of Methanol Dehydration to Dimethyl Ether. Methanol dehydration catalysis occurs via an associative mechanism on MFI zeolites (433 K, 0.01-60 kPa MeOH),⁴⁸ which proceeds via adsorption of gaseous methanol at Brønsted acid sites to form hydrogen-bonded methanol monomers, followed by adsorption of a second methanol to form protonated dimers that rearrange to form dimethyl ether and water. Periodic density functional theory calculations (DFT) calculations show the most abundant reactive intermediates during methanol dehydration catalysis under these conditions (433 K, >0.2 kPa CH₃OH) are methanol monomers and protonated dimers. ⁴⁸ In situ IR spectra (415-433 K, 0.2-16 kPa CH₃OH) of Al-MFI has shown the presence of hydrogen bonding modes for methanol monomers (2380 cm⁻¹) and protonated dimers (~2620 cm⁻¹)⁴⁹ characteristic of associative and dissociative pathways but no surface methoxy species (~1457 cm⁻¹) that are involved in the dissociative pathway.^{29,49} The Langmuirian rate expression derived for associative dehydration where methanol monomers and protonated dimers are the MARI, and DME formation is the kinetically relevant step, is given by

$$r = \frac{k_{\text{first,A}} P_{\text{CH}_3\text{OH}}}{1 + \frac{k_{\text{first,A}}}{k_{\text{zero,A}}} P_{\text{CH}_3\text{OH}}}$$
(3)

In this expression, $k_{\rm first,A}$ and $k_{\rm zero,A}$ are apparent rate constants for kinetic regimes when methanol monomers and protonated dimers are the MARI, respectively.

First-order rate constants reflect the free energy difference between hydrogen-bonded methanol monomers and the transition state that differ in relative size and charge, while zero-order rate constants reflect the difference between the protonated dimers and the same transition state of similar size and charge as the dimer. This renders zero-order rate constants primarily sensitive to differences in acid strength and essentially independent of the local confining environment, because of the similar size of DME formation transition states and protonated methanol dimer intermediates, while the firstorder rate constant is sensitive to both acid strength and confinement. 48,50 Prior reports from our group show first- and zero-order rate constants (per H_{Al}+, 415 K), along with corresponding activation enthalpies and entropies, that are in quantitative agreement with those reported by Jones et al. (per H_{Al}⁺, 433 K)²⁵ for a suite of commercially sourced Al-MFI zeolites. DME formation rates on H-B-Al-MFI (415 K) predominantly reflect contributions from protons that charge compensate framework Al, as evidenced by zero-order rate constants (per H⁺_{Al}) that are similar to those on Al-MFI, allowing for quantitative comparison of DME formation rates between Al-MFI and B-Al-MFI zeolites.22

DME formation rates were measured on four B-Al-MFI zeolites (415 K) and normalized by the number of protons at Al heteroatoms (H⁺_{Al}), as quantified by selective titration with NH₃ (Table 1). Turnover rates increased linearly at low methanol partial pressures (<1 kPa) before approaching a zeroorder dependence at higher pressures (>20 kPa), consistent with previous reports on Al-MFI^{25,29} and B-Al-MFI²² zeolites. Zero- and first-order rate constants (415 K, per H⁺_{Ab}, Table S3) for the samples studied here are plotted as a function of H+Al content in Figure 9 along with those for a series of commercial Al-MFI samples reported previously²⁵ and B-Al-MFI samples synthesized in the presence of TPA+ and EDA reported previously.²² Zero-order rate constants were similar among all B-Al-MFI samples studied here and in quantitative agreement with values previously reported for Al-MFI (433 K, 0-20 kPa CH₃OH;²⁵ 415 K, 0-60 kPa CH₃OH),²⁹ providing validation for the NH₃ titration techniques to selectively quantify H_{Al} sites in B-Al-MFI zeolites and that protons of equivalent acid strength that charge-compensate framework Al contribute predominantly to measured DME formation rates.

First-order rate constants reflect the acid strength of protons and the local void geometry around active sites in MFI zeolites, as the larger transition state is preferentially stabilized over methanol monomers. Higher rate constants indicate confinement within smaller voids as a consequence of van der Waals interactions between the oxide lattice and organic guests. First-order rate constants on B–Al–MFI zeolites (Si/Al ~ 50) were comparable to those on commercial Al–MFI materials previously reported (Figure 9)²⁹ and did not trend systematically with B content, synthesis method, or the fraction of Al counted by Co²⁺ titration (Table S3). Additionally, these rates were not affected by intracrystalline mass transfer limitations, as evidenced by effectiveness factors close to unity (Figure S14) estimated with first-order rate constants and physiochemical properties (Table S3) similar to prior reports. ^{22,29}

Previously reported first-order rate constants on B–Al–MFI were lower and closer to a value of $\sim 2.0 \times 10^{-3}$ mol DME

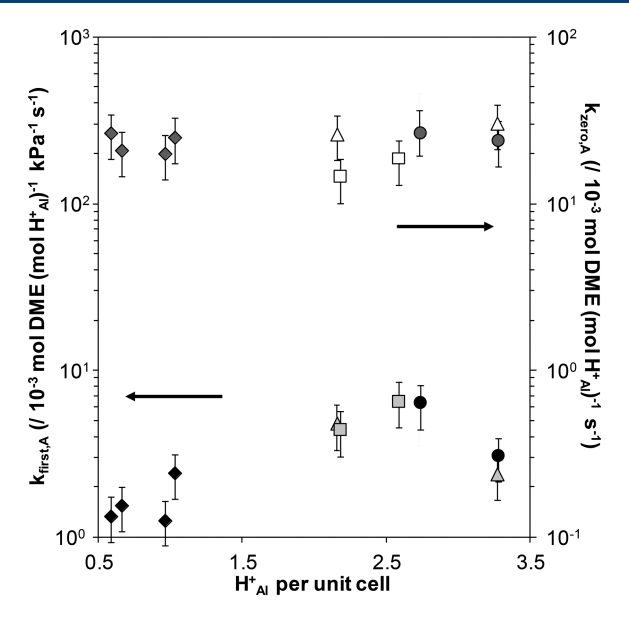


Figure 9. First- and zero-order rate constants of methanol dehydration (415 K) on MFI samples. Samples crystallized in this study in the presence of TPA⁺ (triangles) or a mixture of TPA⁺ and EDA (circles), and previously reported B–Al–MFI samples crystallized with TPA⁺ and EDA at lower Al content (diamonds)²² and commercially available Al–MFI (squares).²⁹ Adapted with permission from ref 22. Copyright 2018 American Chemical Society.

(mol H_{Al}^{+})⁻¹ kPa⁻¹ s⁻¹, which is characteristic of a confining environment of approximately 0.8 nm in diameter. These lower first-order rate constants on B–Al–MFI (Si/Al = 74–153) were interpreted as the preferential siting of Al in MFI channel intersections (~0.7 nm in diameter) compared to the sinusoidal and straight channels (~0.55 nm in diameter). This was attributed to the occlusion of EDA-B complexes in MFI channels, which may bias Al incorporation to T-sites in larger intersections. At higher Al content reported here, the preferential siting of Al at T-sites accessible via channel intersections may be disrupted, as evidenced by first-order rate constants that are between those predicted for protons confined within 0.55 or 0.70 nm diameter voids, consistent with the commercial Al–MFI samples studied previously. ^{25,29}

4. CONCLUSIONS

The methods reported herein provide a strategy to crystallize MFI zeolites containing B and Al heteroatoms with independent influence over bulk zeolite properties (elemental composition, crystallite size) and active site arrangements, defined as Al in isolated or proximal framework locations. The addition of B heteroatoms to MFI synthesis solutions of fixed Al content decreases characteristic crystallite sizes when either TPA+ or mixtures of EDA and TPA+ are used as organic SDAs. This observation may reflect different relative rates of nucleation, growth, and dissolution during hydrothermal synthesis, influenced by the alkalinity of synthetic solutions that are less basic with the addition of boric acid precursors, and the ability of EDA to modify MFI crystallite growth rates. While crystallite sizes are predominantly influenced by Si/B ratios in the synthesis solutions, protons at B heteroatoms are irrelevant for most Brønsted acid-catalyzed reactions, and thus would not contribute to characteristic diffusion parameters that range from $0.2-42 \times 10^{-6}$ mol H⁺_{Al} nm⁻¹ among MFI zeolites synthesized in this work.

The percentage of Al heteroatoms in proximal configurations was measured with Co2+ saturation via liquid phase ion exchange at 353 K in a 0.5 M Co(NO₃)₂ solution for 24 h, and these procedures were validated by cation site balances and UV-visible spectra to verify a 2:1 replacement of monovalent cations by Co²⁺ and the absence of Co-oxide phases, respectively. Using only TPA+ as an organic SDA during B-Al-MFI synthesis (Si/Al \sim 50) resulted in 20-40% of Al located in proximal configurations, irrespective of B content or crystallite size. B-Al-MFI zeolites of similar Al content, but instead crystallized from EDA/TPA+ mixtures, contain <5% of Al in proximal configurations, again independent of B content and crystallite size. While one TPA+ molecule is occluded per channel intersection in MFI zeolites crystallized using only TPA+, those crystallized with $EDA/TPA^{+} = 15$ and excess Si relative to TPA^{+} , as required for substitution of all silicate precursors in TPA+ clathrates (Si/ $TPA^+ > 24$), result in occlusion of approximately one TPA^+ for every two channel intersections. Intracrystalline voids not occupied by TPA+ contain EDA, and EDA-B complexes incorporate two B heteroatoms per EDA with increasing B concentrations in synthesis solutions.

Ammonia titration methods can discriminate between protons at framework Al and B heteroatoms, and catalytic turnovers occur predominantly at the former protons that have lower deprotonation energies. This is demonstrated with methanol dehydration catalysis (415 K, per H⁺_{Al}) in first- and zero-order kinetic regimes, as previously shown for boroaluminosilicates. We propose that these titrations could be used to normalize site-time yields and turnover numbers during hydrocarbon reactions catalyzed by Brønsted acid sites (e.g., methanol-to-hydrocarbons, alkene oligomerization) to decouple the effects of intracrystalline residence times imparted by characteristic diffusion parameters and reactivity differences between active site ensembles in MFI zeolites.

ASSOCIATED CONTENT

S Supporting Information

The Supporting Information is available free of charge on the ACS Publications website at DOI: 10.1021/acs.iecr.9b01726.

X-ray diffraction patterns, nitrogen adsorption isotherms, ^{11}B and ^{27}Al MAS NMR spectra, SEM micrographs, Co^{2+} ion-exchange isotherms, DRUV–visible absorption spectra of Co-MFI, and methanol dehydration kinetics on B–Al–MFI zeolites (PDF)

AUTHOR INFORMATION

Corresponding Author

*E-mail: rgounder@purdue.edu.

ORCID @

Jeffrey T. Miller: 0000-0002-6269-0620 Rajamani Gounder: 0000-0003-1347-534X

Author Contributions

[†]Y.G.H. and P.M.K. contributed equally to this work.

Notes

The authors declare no competing financial interest.

■ ACKNOWLEDGMENTS

We acknowledge the support for this work provided by the National Science Foundation under Cooperative Agreement No. EEC-1647722, an Engineering Research Center for the

Innovative and Strategic Transformation of Alkane Resources (CISTAR). We thank Laura Wilcox for assistance collecting methanol dehydration kinetic data, and for technical discussions and feedback on this manuscript. We also thank John Harwood (Purdue Interdepartmental NMR Facility) for assistance collecting NMR spectra.

REFERENCES

- (1) Degnan, T. F. The Implications of the Fundamentals of Shape Selectivity for the Development of Catalysts for the Petroleum and Petrochemical Industries. *J. Catal.* **2003**, 216, 32–46.
- (2) Gounder, R.; Iglesia, E. The Catalytic Diversity of Zeolites: Confinement and Solvation Effects within Voids of Molecular Dimensions. *Chem. Commun.* **2013**, *49*, 3491–3509.
- (3) Eder, F.; Stockenhuber, M.; Lercher, J. A. Brønsted Acid Site and Pore Controlled Siting of Alkane Sorption in Acidic Molecular Sieves. *J. Phys. Chem. B* **1997**, *101*, 5414–5419.
- (4) Chen, N. Y.; Garwood, W. E. Some Catalytic Properties of ZSM-5, a New Shape Selective Zeolite. *J. Catal.* **1978**, *52*, 453–458.
- (5) Chang, C. D. Hydrocarbons from Methanol. *Catal. Rev.: Sci. Eng.* 1983, 25, 1–119.
- (6) Garwood, W. E. Conversion of C2 -C10 to Higher Olefins over Synthetic Zeolite ZSM-5. ACS Symp. Ser. 1983, 218, 383-396.
- (7) Tabak, S. A. Oligomerization of Olefins. U.S. Patent US4254296A, March 3, 1981.
- (8) Guisnet, M.; Costa, L.; Ribeiro, F. R. Prevention of Zeolite Deactivation by Coking. *J. Mol. Catal. A: Chem.* **2009**, *305*, 69–83.
- (9) Corma, A.; Martínez, C.; Doskocil, E. Designing MFI-Based Catalysts with Improved Catalyst Life for C3= and C5= Oligomerization to High-Quality Liquid Fuels. *J. Catal.* **2013**, 300, 183–196.
- (10) Khare, R.; Millar, D.; Bhan, A. A Mechanistic Basis for the Effects of Crystallite Size on Light Olefin Selectivity in Methanol-to-Hydrocarbons Conversion on MFI. *J. Catal.* **2015**, *321*, *23*–31.
- (11) Khare, R.; Liu, Z.; Han, Y.; Bhan, A. A Mechanistic Basis for the Effect of Aluminum Content on Ethene Selectivity in Methanol-to-Hydrocarbons Conversion on HZSM-5. *I. Catal.* **2017**, 348, 300–305.
- (12) Sarazen, M. L.; Doskocil, E.; Iglesia, E. Effects of Void Environment and Acid Strength on Alkene Oligomerization Selectivity. *ACS Catal.* **2016**, *6*, 7059–7070.
- (13) Cundy, C. S.; Lowe, B. M.; Sinclair, D. M. Crystallisation of Zeolitic Molecular Sieves: Direct Measurements of the Growth Behaviour of Single Crystals as a Function of Synthesis Conditions. *Faraday Discuss.* **1993**, *95*, 235–252.
- (14) Persson, A. E.; Schoeman, B. J.; Sterte, J.; Otterstedt, J. E. Synthesis of Stable Suspensions of Discrete Colloidal Zeolite (Na, TPA)ZSM-5 Crystals. *Zeolites* **1995**, *15*, 611–619.
- (15) Chang, C. D.; Bell, A. T. Studies on the Mechanism of ZSM-5 Formation. *Catal. Lett.* **1991**, *8*, 305–316.
- (16) de Ruiter, R.; Jansen, J. C.; van Bekkum, H. On the Incorporation Mechanism of B and AI in MFI-Type Zeolite Frameworks. *Zeolites* **1992**, *12*, 56–62.
- (17) Yokoi, T.; Mochizuki, H.; Namba, S.; Kondo, J. N.; Tatsumi, T. Control of the Al Distribution in the Framework of ZSM-5 Zeolite and Its Evaluation by Solid-State NMR Technique and Catalytic Properties. *J. Phys. Chem. C* **2015**, *119*, 15303–15315.
- (18) Lupulescu, A. I.; Rimer, J. D. Tailoring Silicalite-1 Crystal Morphology with Molecular Modifiers. *Angew. Chem.* **2012**, *124*, 3401–3405.
- (19) Rimer, J. D. Zeolite Compositions and Methods for Tailoring Zeolite Crystal Habits with Growth Modifiers. World Patent No. WO2012106675A2, August 9, 2012.
- (20) Gunawardane, R. P.; Gies, H.; Marler, B. Long-Chain Polyamines and Amine-Boric Acid Pairs as Templates for the Synthesis of Porous Tectosilicates. *Zeolites* **1988**, *8*, 127–131.
- (21) Perego, G.; Bellussi, G.; Millini, R.; Alberti, A.; Zanardi, S. B-Containing Molecular Sieves Crystallized in the Presence of

- Ethylenediamine. Part II: Crystal Structure of as-Synthesized B-MFI. *Microporous Mesoporous Mater.* **2003**, *58*, 213–223.
- (22) Kester, P. M.; Miller, J. T.; Gounder, R. Ammonia Titration Methods to Quantify Brønsted Acid Sites in Zeolites Substituted with Aluminum and Boron Heteroatoms. *Ind. Eng. Chem. Res.* **2018**, *57*, 6673–6683.
- (23) Chen, J.; Liang, T.; Li, J.; Wang, S.; Qin, Z.; Wang, P.; Huang, L.; Fan, W.; Wang, J. Regulation of Framework Aluminum Siting and Acid Distribution in H-MCM-22 by Boron Incorporation and Its Effect on the Catalytic Performance in Methanol to Hydrocarbons. *ACS Catal.* **2016**, *6*, 2299–2313.
- (24) Chu, C. T. W.; Kuehl, G. H.; Lago, R. M.; Chang, C. D. Isomorphous Substitution in Zeolite Frameworks. II. Catalytic Properties of [B]ZSM-5. *J. Catal.* 1985, 93, 451–458.
- (25) Jones, A. J.; Carr, R. T.; Zones, S. I.; Iglesia, E. Acid Strength and Solvation in Catalysis by MFI Zeolites and Effects of the Identity, Concentration and Location of Framework Heteroatoms. *J. Catal.* **2014**, *312*, 58–68.
- (26) Zhu, Q.; Kondo, J. N.; Yokoi, T.; Setoyama, T.; Yamaguchi, M.; Takewaki, T.; Domen, K.; Tatsumi, T. The Influence of Acidities of Boron- and Aluminium-Containing MFI Zeolites on Co-Reaction of Methanol and Ethene. *Phys. Chem. Chem. Phys.* **2011**, *13*, 14598.
- (27) Baerlocher, C.; McCusker, L. B. Database of Zeolite Structures. http://www.iza-structure.org/databases/. Last accessed June 6, 2019.
- (28) Di Iorio, J. R.; Bates, S. A.; Verma, A. A.; Delgass, W. N.; Ribeiro, F. H.; Miller, J. T.; Gounder, R. The Dynamic Nature of Brønsted Acid Sites in Cu-Zeolites During NOx Selective Catalytic Reduction: Quantification by Gas-Phase Ammonia Titration. *Top. Catal.* 2015, 58, 424–434.
- (29) Di Iorio, J. R.; Nimlos, C. T.; Gounder, R. Introducing Catalytic Diversity into Single-Site Chabazite Zeolites of Fixed Composition via Synthetic Control of Active Site Proximity. *ACS Catal.* **2017**, *7*, 6663–6674.
- (30) Qiao, Q.; Wang, R.; Gou, M.; Yang, X. Catalytic Performance of Boron and Aluminium Incorporated ZSM-5 Zeolites for Isomerization of Styrene Oxide to Phenylacetaldehyde. *Microporous Mesoporous Mater.* **2014**, *195*, 250–257.
- (31) Scholle, K. F. M. G. J.; Veeman, W. S. The Influence of Hydration on the Coordination State of Boron in H-Boralite Studied By¹¹B Magic Angle Spinning n.m.R. *Zeolites* **1985**, *5*, 118–122.
- (32) Koller, H.; Fild, C.; Lobo, R. F. Variable Anchoring of Boron in Zeolite Beta. *Microporous Mesoporous Mater.* **2005**, *79*, 215–224.
- (33) Sayed, M. B.; Auroux, A.; Védrine, J. C. The Effect of Boron on ZSM-5 Zeolite Shape Selectivity and Activity. II. Coincorporation of Aluminium and Boron in the Zeolite Lattice. *J. Catal.* **1989**, *116*, 1–10
- (34) Iwasaki, A.; Sano, T.; Kiyozumi, Y. Effect of Additives on the Growth Behavior of Silicalite Crystal. *Microporous Mesoporous Mater.* 1998, 25, 119–126.
- (35) Dědeček, J.; Kaucký, D.; Wichterlová, B.; Gonsiorová, O. Co²⁺ Ions as Probes of Al Distribution in the Framework of Zeolites. ZSM-5 Study. *Phys. Chem. Chem. Phys.* **2002**, *4*, 5406–5413.
- (36) Dědeček, J.; Kaucký, D.; Wichterlová, B. Co²⁺ Ion Siting in Pentasil-Containing Zeolites, Part 3. Co²⁺ Ion Sites and Their Occupation in ZSM-5: A VIS Diffuse Reflectance Spectroscopy Study. *Microporous Mesoporous Mater.* **2000**, 35–36, 483–494.
- (37) Janda, A.; Bell, A. T. Effects of Si/Al Ratio on the Distribution of Framework Al and on the Rates of Alkane Monomolecular Cracking and Dehydrogenation in H-MFI. *J. Am. Chem. Soc.* **2013**, 135, 19193–19207.
- (38) Li, C.; Vidal-Moya, A.; Miguel, P. J.; Dedecek, J.; Boronat, M.; Corma, A. Selective Introduction of Acid Sites in Different Confined Positions in ZSM-5 and Its Catalytic Implications. *ACS Catal.* **2018**, *8*, 7688–7697.
- (39) Liang, T.; Chen, J.; Qin, Z.; Li, J.; Wang, P.; Wang, S.; Wang, G.; Dong, M.; Fan, W.; Wang, J. Conversion of Methanol to Olefins over H-ZSM-5 Zeolite: Reaction Pathway Is Related to the Framework Aluminum Siting. ACS Catal. 2016, 6, 7311–7325.

- (40) Pashkova, V.; Klein, P.; Dedecek, J.; Tokarová, V.; Wichterlová, B. Incorporation of Al at ZSM-5 Hydrothermal Synthesis. Tuning of Al Pairs in the Framework. *Microporous Mesoporous Mater.* **2015**, 202, 138–146
- (41) Nagy, J. B.; Gabelica, Z.; Derouane, E. G. Position and Configuration of the Guest Organic Molecules within the Framework of the ZSM-5 and ZSM-11 Zeolites. *Zeolites* **1983**, *3*, 43–49.
- (42) Cornaro, U.; Wojciechowski, B. W. The Catalytic Effect of Boron Substitution in ZSM-5 Type Zeolites. *J. Catal.* **1989**, 120, 182–101
- (43) Wang, S.; Wang, P.; Qin, Z.; Chen, Y.; Dong, M.; Li, J.; Zhang, K.; Liu, P.; Wang, J.; Fan, W. Relation of Catalytic Performance to the Aluminum Siting of Acidic zeolites in the Conversion of Methanol to Olefins, Viewed via a Comparison between ZSM-5 and ZSM-11. ACS Catal. 2018, 8, 5485–5505.
- (44) Symons, M. C. R. Water Structure and Reactivity. Acc. Chem. Res. 1981, 14, 179–187.
- (45) de Ruite, R.; Famine, K.; Kentgens, A. P. M.; Jansen, J. C.; van Bekkum, H. Synthesis of Molecular Sieve [B]-BEA and Modification of the Boron Site. *Zeolites* **1993**, *13*, 611–621.
- (46) Chawla, A.; Li, R.; Jain, R.; Clark, R. J.; Sutjianto, J. G.; Palmer, J. C.; Rimer, J. D. Cooperative effects of inorganic and organic structure-directing agents in ZSM-5 crystallization. *Mol. Syst. Des. Eng.* **2018**, *3*, 159–170.
- (47) Testa, F.; Chiappetta, R.; Crea, F.; Aiello, R.; Fonseca, A.; Nagy, J. B. Synthesis of Borosilicalite-1 with High Boron Content from Fluoridecontaining Media. *Stud. Surf. Sci. Catal.* **1995**, *94*, 349–356
- (48) Carr, R. T.; Neurock, M.; Iglesia, E. Catalytic Consequences of Acid Strength in the Conversion of Methanol to Dimethyl Ether. *J. Catal.* **2011**, 278, 78–93.
- (49) Jones, A. J.; Iglesia, E. Kinetic, Spectroscopic, and Theoretical Assessment of Associative and Dissociative Methanol Dehydration Routes in Zeolites. *Angew. Chem., Int. Ed.* **2014**, *53*, 12177–12181.
- (50) Jones, A. J.; Zones, S. I.; Iglesia, E. Implications of Transition State Confinement within Small Voids for Acid Catalysis. *J. Phys. Chem. C* **2014**, *118*, 17787–17800.